The Astrophysical Journal, 887:18 (11pp), 2019 December 10 https://doi.org/10.3847/1538-4357/ab4ceb

Classification of New X-Ray Counterparts for *Fermi* Unassociated Gamma-Ray Sources Using the *Swift* X-Ray Telescope

Amanpreet Kaur[1], Abraham D. Falcone[1], Michael D. Stroh[2], Jamie A. Kennea[1], and Elizabeth C. Ferrara[3,4]
[1] The Pennsylvania State University, 525 Davey Lab, University Park, PA 16802, USA
[2] Center for Interdisciplinary Exploration and Research in Astrophysics (CIERA), Northwestern University, Evanston, IL 60208, USA
[3] NASA Goddard Space Flight Center, Greenbelt, MD 20771, USA
[4] Department of Astronomy, University of Maryland College Park, MD 20742, USA
Received 2019 August 21; revised 2019 October 8; accepted 2019 October 9; published 2019 December 5

Abstract

Approximately one-third of the gamma-ray sources in the third *Fermi*-LAT catalog are unidentified or unassociated with objects at other wavelengths. Observations with the X-Ray Telescope on the *Neil Gehrels Swift Observatory* (*Swift*-XRT) have yielded possible counterparts in ∼30% of these source regions. The objective of this work is to identify the nature of these possible counterparts, utilizing their gamma-ray properties coupled with the *Swift* derived X-ray properties. The majority of the known sources in the *Fermi* catalogs are blazars, which constitute the bulk of the extragalactic gamma-ray source population. The galactic population on the other hand is dominated by pulsars. Overall, these two categories constitute the majority of all gamma-ray objects. Blazars and pulsars occupy different parameter space when X-ray fluxes are compared with various gamma-ray properties. In this work, we utilize the X-ray observations performed with the *Swift*-XRT for the unknown *Fermi* sources and compare their X-ray and gamma-ray properties to differentiate between the two source classes. We employ two machine-learning algorithms, decision tree and random forest (RF) classifier, to our high signal-to-noise ratio sample of 217 sources, each of which corresponds to *Fermi* unassociated regions. The accuracy scores for both methods were found to be 97% and 99%, respectively. The RF classifier, which is based on the application of a multitude of decision trees, associated a probability value ($P_{\rm bzr}$) for each source to be a blazar. This yielded 173 blazar candidates from this source sample, with $P_{\rm bzr} \geqslant 90\%$ for each of these sources, and 134 of these possible blazar source associations had $P_{\rm bzr} \geqslant 99\%$. The results yielded 13 sources with $P_{\rm bzr} \leqslant 10\%$, which we deemed as reasonable candidates for pulsars, seven of which result with $P_{\rm bzr} \leqslant 1\%$. There were 31 sources that exhibited intermediate probabilities and were termed ambiguous due to their unclear characterization as a pulsar or a blazar.

Unified Astronomy Thesaurus concepts: Gamma-ray sources (633); Blazars (164); Pulsars (1306); X-ray sources (1822)

1. Introduction

Since the launch of the *Fermi* Gamma Ray Space Telescope in 2008 June, thousands of gamma-ray sources have been discovered in our universe. Four point-source catalogs have been published to-date, with 1451 sources in the 1FGL (Abdo et al. 2010) catalog, 1873 sources in the 2FGL (Nolan et al. 2012) catalog, and 3033 sources in the 3FGL (Acero et al. 2015) catalog; as well as 5065 sources in the recently released 4FGL, which is too recent to be considered in the multiwavelength follow-up and classification effort that is described in this paper. The dominant source classes in all of these catalogs are blazars and pulsars, representing the extragalactic and galactic sky, respectively. Other classes include X-ray binaries, gamma-ray bursts, supernova remnants, globular clusters, starburst galaxies, etc. Most of the sources in the 1FGL and 2FGL catalogs are also present in the 3FGL catalog, with much improved measurements (∼2.′5 uncertainty). While some of these sources are attributed to one or the other class, about one-third (1010) are unassociated and unidentified. A rather large fraction of the known gamma-ray sources are blazars (75%), therefore it is highly likely that some of the unassociated ones could belong to a fainter subclass of blazars. Finding these blazars would offer an opportunity to conduct the population studies in a complete manner, thereby shedding light on the still debated idea of a blazar sequence (Fossati et al. 1998; Ghisellini et al. 2017). In addition to blazars, some previous studies of unassociated sources from *Fermi* catalogs have led to discoveries of millisecond pulsars, black widows, redback pulsars, high-mass X-ray binaries, and extreme blazars; e.g., see Saz Parkinson et al. (2010) and Ransom et al. (2011). The emission processes of these newly discovered objects are still not completely understood and are an active field of research. Furthermore, some of these objects could potentially be the candidates for a new class of gamma-ray sources, which could help to uncover new and extreme astrophysical environments that could possibly contribute to studies of new physics. Overall, finding the nature of these mysterious gamma-ray sources is critical for furthering our understanding of gamma-ray blazar and pulsar systems, as well as possible new source classes, and for the study of the gamma-ray sky and the extreme environments that illuminate it. Finding and classifying multiwavelength counterpart sources is a logical first step in this process.

In the past, Massaro et al. (2012) developed a technique, further refined by D'Abrusco et al. (2013) which utilized *WISE* (Sharma & Chauhan 2011) colors to differentiate blazars from other source populations. However, to identify both pulsars and blazars, various machine-learning algorithms were successfully employed utilizing the *Fermi*-LAT gamma-ray data, e.g., see Saz Parkinson et al. (2016) and Lefaucheur & Pita (2017). In this work, we attempt to characterize the new potential associations for the 3FGL unassociated sources that have been found by A. D. Falcone et al. (2019, in preparation) by applying machine-learning algorithms to their X-ray and gamma-ray parameters obtained from *Fermi* and *Swift*-XRT observations of these regions, respectively. The reason for utilizing X-ray observations is based on the fact that the gamma-ray and X-ray bands are close enough in energy space to share many of the same types of high-energy emitters as their source populations. Moreover, the X-ray observations with *Swift* reduces the positional uncertainty of these *Fermi* sources from a few arcminutes to a few arcseconds, thereby making the identification process much easier. More importantly, pulsars and blazars occupy different parameter space when X-ray fluxes are compared (Falcone et al. 2015), which makes it a crucial parameter for machine-learning algorithms to classify sources as blazars or pulsars. The structure of this paper is described as follows: Section 2 describes the observational details and sample selection criteria. In addition, the details of analysis procedure are explained in this section. Section 3 describes our findings by comparing gamma-ray and X-ray properties of our sample. In Section 3.1, we introduce machine-learning methods employing gamma-rays and X-rays to classify these objects as blazars or pulsars. A detailed discussion of our conclusions is provided in Section 5.

2. Observations and Analysis

A sample of unidentified objects from the 3FGL catalog were selected for observations with *Swift*-XRT through *Swift* fill-in and GI programs to find potential X-ray counterparts. Detailed information about the sample selection, observations, and analysis methods can be found in A. D. Falcone et al. (2019, in preparation). One of the selection criteria for this sample was based on the desire to contain the confidence regions of the 3FGL sources within the field of view of *Swift*-XRT. Therefore, the sources with position confidence region semimajor axes $<10'$ were selected. At the time of this writing, the total sample included 803 targeted 3FGL positions. The exposure time for each source was typically $\sim$4 ks.

From the 803 unassociated *Fermi* sources that were observed, at least one X-ray source was detected in 552 of the the 95% uncertainty regions. For this study, the following two selection criteria were utilized: (i) only the objects with detections at the significance threshold of signal-to-noise ratio $\geqslant$4, and (ii) the sources with only one X-ray counterpart within the 95% *Fermi* confidence region were selected. This led to a total of 217 X-ray sources found within the 95% confidence regions of 217 *Fermi* unassociated sources. The complete details of these 217 sources are provided in A. D. Falcone et al. (2019, in preparation).

3. Methods

The 3FGL catalog is comprised of blazars, pulsars, supernova remnants, starburst galaxies, gamma-ray bursts, globular clusters, etc., among the known classes of astrophysical sources. However, blazars and pulsars dominate the extragalactic and galactic source class populations, constituting $\sim$75% and $\sim$8% of the total sources, respectively. Therefore, it is highly likely that a majority of the unknown sources are potentially blazars or pulsars. Falcone et al. (2015) demonstrated that blazars and pulsars occupy different parameter space when gamma-ray properties are compared with X-ray fluxes. We investigate this scenario by comparing the gamma-ray and X-ray properties of the unassociated sources with that of the known blazars and pulsars.

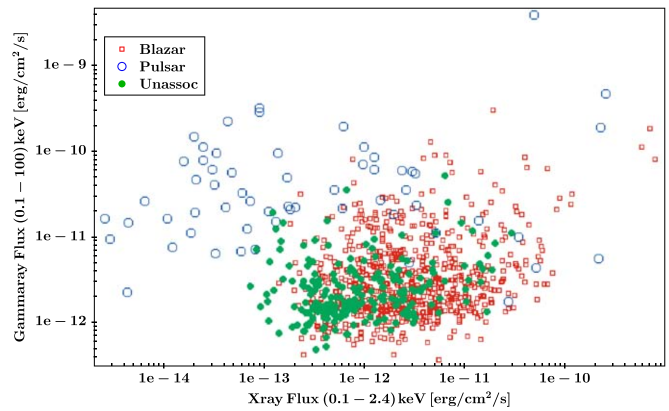

Figure 1. X-ray vs. gamma-ray flux from known blazars (red) and pulsars (blue). The 217 unassociated sources (green) are plotted over the same space.

The first step was to conduct a search for blazars and pulsars in the literature for which both gamma-ray and X-ray data were available. Gamma-ray properties for all the known sources, i.e., known blazars and pulsars were derived from the 3FGL catalog. The X-ray flux values for blazars were acquired from the 3LAC catalog (Ackermann et al. 2015), whereas for pulsars, X-ray fluxes were obtained from Marelli (2012), Pryal (2015, and references therein), Saz Parkinson et al. (2016), Wu et al. (2018), Zyuzin et al. (2018), and the *Swift*-XRT archive (See Appendix for details on this analysis). This resulted in a sample size of 753 sources: 691 blazars and 59 pulsars for which both gamma-ray data as well as typical X-ray flux were available. The number of pulsars we found in the literature for which gamma-ray and X-ray observations were present relevant to this work were rather small in number as compared to blazars. 38 of these pulsars are young, 4 are middle aged, and 17 are millisecond pulsars. For 217 sources in the unassociated sample, the *Swift*-XRT count rate was converted to X-ray flux assuming an absorbed power-law spectrum with spectral index 2.0 employing PIMMS[5] tool (Mukai 1993). For each source, the neutral hydrogen column density was calculated using the HEASARC N_H calculator.[6]

The typical X-ray fluxes for pulsars are about 10–10,000 times lower than gamma-ray fluxes (Marelli et al. 2011), which provides the preliminary discrimination for blazars and pulsars, as shown in Figure 1. Moreover, the overall shape of spectral energy distribution of pulsars are more curved than blazars, which provides yet another factor for this difference, e.g., see Figure 2. This separation can also be seen when one compares other gamma-ray properties, such as spectral indices and variability indices, as demonstrated in Figures 3 and 4, respectively.

While a comparison between gamma-ray and X-ray properties of blazars and pulsars does allow one to distinguish blazars from pulsars in a two parameter space environment, a more robust analysis is desired in order to combine all these parameters and utilize them simultaneously for the discrimination between the two dominant classes. For this purpose, we applied two machine-learning classifiers as described below in Section 3.1.

[5] https://heasarc.gsfc.nasa.gov/docs/software/tools/pimms.html
[6] https://heasarc.gsfc.nasa.gov/cgi-bin/Tools/w3nh/w3nh.pl

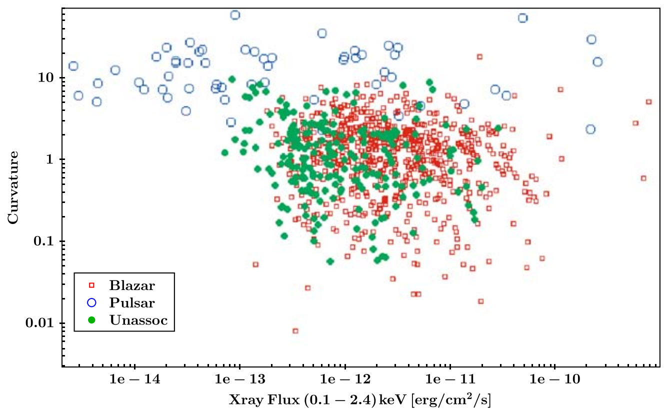

Figure 2. X-ray flux vs. curvature index from known blazars (red) and pulsars (blue). The 217 unassociated sources (green) are plotted over the same space.

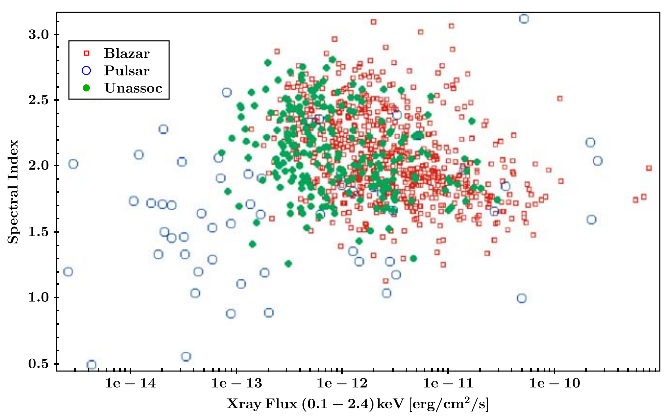

Figure 3. X-ray flux vs. spectral index from known blazars (red) and pulsars (blue). The 217 unassociated sources (green) are plotted over the same space.

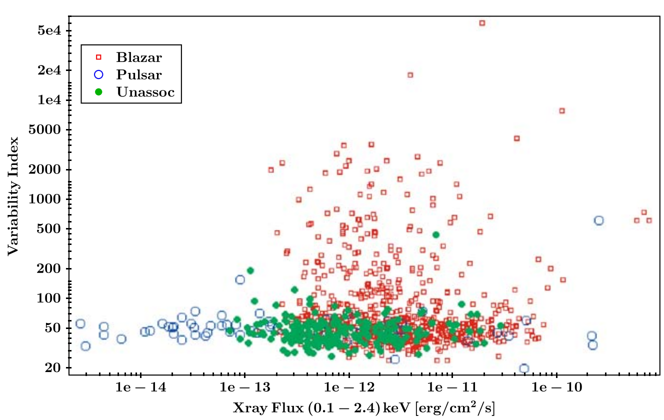

Figure 4. X-ray flux vs. variability index from known blazars (red) and pulsars (blue). The 217 unassociated sources (green) are plotted over the same space.

3.1. Classification with Machine Learning

In the last decade, although the number of gamma-ray sources has increased by a substantial amount, the number of sources with no classification has also increased. One of the best approaches to classify these objects is to obtain multi-wavelength data to create complete spectral energy distributions and thereby study their properties in a detailed manner. This kind of work requires multiple years of investigation, thereby making it inefficient with respect to time. Recently, the big data revolution in astrophysics has motivated the community to start applying machine-learning techniques for classification purposes, e.g., Ackermann et al. (2012), Mirabal et al. (2012, 2016), Saz Parkinson et al. (2016), Salvetti et al. (2017), and Chiaro et al. (2016) applied various machine-learning classifiers in the context of *Fermi* unidentified sources. Among all the methods employed by these authors, the random forest (RF) classifier (Breiman 2001) yielded results with accuracy >95%. We therefore utilize an RF classifier technique for the classification purpose in this work. For comparison and verification of the RF results, we employed another method called decision tree (DT; Quinlan & Shapiro 1990), which is based on the same principle as the former method. A brief explanation of both methods is provided below.

3.1.1. Decision Tree

A decision tree (DT) classifier is an example of a nonparametric supervised machine-learning method. It utilizes multiple given parameters to distinguish between classes by branching these parameters, one at a time, into different nodes and thereby labeling a source to one or the other class. This decision of branching/splitting is based on an index called the Gini impurity index. This index represents the probability for a source to be assigned a wrong label/class, given it is chosen randomly from the given data set. The nodes in the decision tree are split until a Gini impurity reaches its minimum, and at this stage, a source is labeled with the correct class. This algorithm was employed through `sklearn 0.20.3` which is available in Python3.7.3.

3.1.2. Random Forest

The RF method is the most commonly employed supervised technique for classification purposes. The underlying principle for RF is the decision tree method described above. The main difference in this case is that RF employs a multitude of decision trees instead of relying on the results of one such tree. The final source class is defined by taking an aggregate of the results from all these decision trees. Because this method is based on taking an average of multiple decision tree algorithms, it provides a more robust analysis and also solves the problem of overfitting, which is commonly seen in DT methods. We used this method using `sklearn 0.20.3` which is available in Python3.7.3. utilizing 1000 decision trees and Gini inequality as the criteria for splitting the nodes for classification. The minimum number of nodes were set to 1. The application of these two methods and their results are discussed below.

3.2. Training and Test Samples

First, the total sample (774 sources) of known blazars and pulsars for which we have *Fermi* and X-ray data were divided into training and test samples; the combined training plus test sample contained 710 blazars and 64 pulsars with known characteristics. The training data set contained 669 sources: 620 blazars and 49 pulsars. The rest of the 100 sources (90 blazars and 10 pulsars) were assigned to the test sample. The purpose of dividing the known sources into two samples is to check the accuracy of each method through the test sample after the classifier is trained on the training sample. The five parameters chosen for classification purposes were gamma-ray flux, X-ray flux, gamma-ray spectral index, gamma-ray variability index, and curvature. These properties have already shown promise for distinguishing blazars from pulsars, as explained in Section 3. Since the training sample is obviously biased toward one class (blazars), we employed a method called SMOTE (synthetic minority over-sampling technique; Chawla et al. 2002), which generates synthetic data points for the under-represented class using the k-nearest neighbors algorithm, choosing six as the number of nearest neighbors. We employed this algorithm utilizing Python 3.7.3. After employing this method, the training set constituted 620 blazars and 620 pulsars. In the next step, both the DT and RF classifiers were run on this training set, independently. The trainer classifiers in each case were then applied to the test sample, which yielded an accuracy of 97% and 99% in the DT and RF cases, respectively.

4. Classification Results

The trained classifiers from both methods were finally applied to the sample of 217 X-ray sources, which yielded 39 candidate pulsars and 178 candidate blazars according to the single iteration of a DT classifier. The RF classifier, which was based on 1000 DT iterations, predicted 13 likely pulsar candidates and 173 likely blazar candidates, assuming the sources with blazar probabilities ⩾90% are blazars and the ones with blazar probabilities ⩽10% are pulsars. The sources with $P_{\rm bzr} \geqslant 99\%$ and ⩽1% are termed as blazar candidates and pulsar candidates, respectively. See Table 1 for details. The rest of the sources exhibiting "ambiguous" classification (31 in number), with blazar probabilities between 10% and 90%, are listed in Table 2. The probability results from the RF classifier as well as our classification based on these probabilities are provided in each table. A receiver operating characteristic (ROC) curve, which displays the true positive rate versus false positive rate at various thresholds was constructed for both the methods. An ROC curve following a path closer to the left-hand border (small false positive rate) and then the top border (true positive rate 1) would represent an ideal method with 100% accuracy. In our case, RF yields slightly better accuracy than the DT method. See Figure 5 for a comparison. In addition, confusion matrices were generated for both the methods. A confusion matrix provides a visualization of the performance of the underlying algorithm provided true classification is known for that data set. (see Figure 6 for details). We emphasize that the results form a random classifier that is the iteration of 1000 decision trees, which is more robust compared to a single decision tree run for classification as can be seen from both ROCs as well as confusion matrices.

Since the release of the 3FGL catalog, various independent studies led to identification/characterization of some of these sources. In particular, various optical spectroscopic campaigns, such as Sandrinelli et al. (2013), Massaro et al. (2016), Crespo et al. (2016a), Peña-Herazo et al. (2017), and Paiano et al. (2017a, 2017b, 2018b) associated 56 of these sources with QSOs, BL Lac objects, and Seyfert type 2 galaxies. Several others were identified as pulsars or pulsar candidates through multiwavelength techniques and machine-learning methods, respectively. In addition, the 4FGL catalog (Collaboration 2019) has been released this year which has identified 42

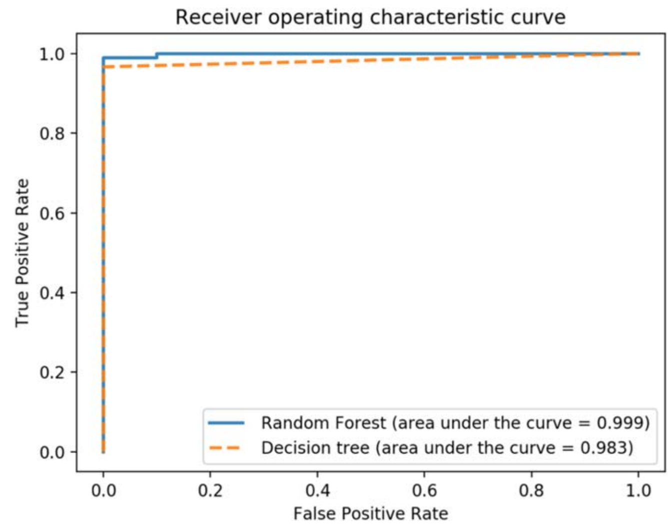

Figure 5. ROC curve for test samples of both the decision tree and random forest classifier for comparison. It is clearly seen that the latter provides better accuracy in the classification results. In addition, the respective areas under the curve are shown in the legend for both methods.

sources from our sample: seven BL Lacertae objects, seven FSRQs (flat spectrum radio quasars), six pulsars, and 22 BCUs (blazar candidates of uncertain type) among these unassociated sources. See column 5 of Tables 1 and 2 and for details of these findings. Please note that all the possible classifications resulting from our machine-learning algorithms with associated probabilities ⩾99% or ⩽1% are consistent with the results from independent studies. However, we note that two *Fermi* sources, 3FGL J0158.6+0102 and 3FGL J1322.3+0839, have been identified as BL Lac objects with an optical spectroscopic survey by Paiano et al. (2017a), whereas they are identified as FSRQs in the 4FGL catalog. In addition, one source, 3FGL J1227.9-4834, which is listed as an ambiguous source according to our classification mechanism, has been previously identified as a low-mass X-ray binary.

4.1. Miscellaneous

Out of the total 217 sources, we found that three sources, 3FGL J0748.8-2208, 3FGL J1624.1-4700, and 3FGL J1801.5-7825, have possible X-ray counterparts that are in positional coincidence with known stars within their respective uncertainties provided by *Swift*-XRT. In the case of 3FGL J1801.5-7825, this star is a K III subgiant, HD162298, which belongs to the category of FK Com stars. These stars are known as X-ray emitters due to their rapid rotation and strong magnetic fields. For 3FGL J1624.1-4700, the positionally coincident star is a rotationally variable star, CD-46 10711. These stars could be associated with the coincident X-ray source, and the source of gamma rays (e.g., as companions in low-mass X-ray binary systems), or the positional overlap of the possibly associated sources could simply be a coincidence. The spectral type of the star, TYC 5993-3722-1, coincident with the *Swift*-XRT position for 3FGL J0748.8-2208 is unknown. It is possible that this star could be a companion in an X-ray binary system or in a coincidental positional overlap with a background blazar (see Table 1).

Table 1
Classification with Machine Learning

Swift Name SwF3	Fermi Name 3FGL	Class	Random Forest Blazar Probability	X-Ray Flux[a] (0.1–2.4) keV	Gamma-Ray Flux[a] (0.1–100) GeV	Notes Classification in Literature
J000132.8-415523	J0002.2-4152	blazar	0.995	23.75	13.11	
J000805.3+145019	J0008.3+1456	blazar	0.999	28.27	16.11	BLL (Paiano et al. 2017a), bcu (4FGL, Collaboration 2019)
J000922.4+503029	J0009.3+5030	blazar	1	4.17	159.34	
J003119.8+072450	J0031.3+0724	blazar	0.999	6.26	15.8	
J003159.9+093616	J0031.6+0938	likely blazar	0.944	4.13	6.79	NLSy1 (Paiano et al. 2017a)
J004859.4+422349	J0049.0+4224	blazar	1	6.91	16.72	BLL (Paiano et al. 2018a)
J011619.9-615343	J0116.3-6153	blazar	0.999	2.86	22.06	
J012152.5-391545	J0121.8-3917	likely blazar	0.971	31.76	11.56	BLL (Peña-Herazo et al. 2017)
J013106.8+612035	J0131.2+6120	blazar	0.993	118.9	118.45	
J013255.1+593213	J0133.3+5930	likely blazar	0.97	12.21	14.38	
J013320.9-441310	J0133.0-4413	blazar	1	3.37	16.41	bll (4FGL, Collaboration 2019)
J013750.3+581411	J0137.8+5813	blazar	0.993	139.6	49.49	
J014347.5-584552	J0143.7-5845	likely blazar	0.977	168.9	62.87	BLL (Landoni et al. 2015)
J015624.4-242003	J0156.5-2423	blazar	1	11.19	11.82	BLL (Peña-Herazo et al. 2017)
J015852.4+010127	J0158.6+0102	blazar	0.991	1.39	7.75	BLL (Paiano et al. 2017a), fsrq (4FGL, Collaboration 2019)
J020020.9-410934	J0200.3-4108	blazar	0.998	8.02	15.75	BLL (Peña-Herazo et al. 2017)
J021210.5+532140	J0212.1+5320	likely pulsar	0.017	10.25	83.78	pulsar (Li et al. 2016)
J022302.7+682158	J0223.3+6820	likely blazar	0.989	19.4	31.75	
J022613.7+093725	J0226.3+0941	likely blazar	0.98	1.23	24.65	fsrq (4FGL, Collaboration 2019)
J023854.1+255406	J0239.0+2555	blazar	0.998	15.6	11.28	BLL (Paiano et al. 2018a)
J025047.7+562935	J0250.6+5630	blazar	0.998	22.41	31.19	
J025111.4-183115	J0251.1-1829	likely blazar	0.967	5.94	13.77	BLL (Paiano et al. 2017a)
J025857.5+055243	J0258.9+0552	blazar	0.996	5.98	26.3	BLL (Paiano et al. 2017a)
J030514.8-160820	J0305.2-1607	blazar	0.997	20.63	16.6	BLL (Paiano et al. 2018a)
J031614.2-643731	J0316.2-6436	blazar	0.997	62.52	31.08	BLL (Landoni et al. 2015)
J033514.0-445945	J0335.3-4459	blazar	0.995	4.99	32.5	
J033829.2+130215	J0338.5+1303	likely blazar	0.964	26.12	53.87	BLL (Paiano et al. 2018a)
J034050.0-242259	J0340.4-2423	blazar	0.999	3	11.64	QSO (Peña-Herazo et al. 2017), bcu (4FGL, Collaboration 2019)
J034819.8+603507	J0348.4+6039	blazar	0.999	101.7	17.85	
J035051.2-281633	J0351.0-2816	blazar	0.999	30.24	10.16	BLL (Peña-Herazo et al. 2017)
J035309.4+565430	J0352.9+5655	blazar	0.996	27.14	37.64	BLL (Crespo et al. 2016b)
J035939.3+764628	J0359.7+7649	blazar	0.994	4.93	10.47	bcu (4FGL, Collaboration 2019)
J040946.5-035958	J0409.8-0358	likely pulsar	0.908	3.13	38.07	BLL (Paiano et al. 2018a)
J041433.2-084214	J0414.9-0840	blazar	0.997	2.12	9.44	BLL (Paiano et al. 2017a)
J042011.0-601505	J0420.4-6013	blazar	0.993	20.01	15.97	BLL (Peña-Herazo et al. 2017)
J042749.8-670435	J0427.9-6704	blazar	0.993	3.91	21.36	
J042958.7-305932	J0430.1-3103	blazar	0.999	7.64	9.56	
J043836.8-732920	J0437.7-7330	likely blazar	0.986	3.69	13.63	
J043949.6-190100	J0439.9-1859	likely blazar	0.985	2.43	26.89	
J044722.5-253937	J0447.1-2540	blazar	0.996	3.04	11.14	BLL (Peña-Herazo et al. 2017), bcu (4FGL, Collaboration 2019)
J045149.6+572141	J0451.7+5722	blazar	0.99	4.45	13.8	
J050650.1+032400	J0506.9+0321	blazar	0.999	6.25	14.99	BLL (Paiano et al. 2017a)
J051641.4+101243	J0516.6+1012	blazar	1	3.95	15.39	
J052140.9+010256	J0521.7+0103	blazar	0.997	1.06	21.69	
J053357.3-375755	J0533.8-3754	likely blazar	0.962	4.24	14.03	fsrq (4FGL, Collaboration 2019)
J055940.6+304233	J0559.8+3042	blazar	0.997	3.2	24.64	
J064847.6+151623	J0648.8+1516	blazar	0.993	197.9	86.49	
J065845.2+063711	J0658.6+0636	blazar	0.995	5.72	20.27	
J070014.4+130425	J0700.2+1304	blazar	0.998	11.38	23.73	BLL (Crespo et al. 2016b)
J070421.7-482645	J0704.3-4828	blazar	0.999	9.9	10.43	
J072547.5-054830	J0725.7-0550	blazar	0.997	24.51	22.69	
J074627.0-022552	J0746.4-0225	blazar	0.998	14.24	31.49	
J074724.8-492634	J0747.5-4927	blazar	0.999	12.47	17.03	BLL (Peña-Herazo et al. 2017)

Table 1
(Continued)

Swift Name SwF3	Fermi Name 3FGL	Class	Random Forest Blazar Probability	X-Ray Flux[a] (0.1–2.4) keV	Gamma-Ray Flux[a] (0.1–100) GeV	Notes Classification in Literature
J074903.8-221016[b]	J0748.8-2208	blazar	0.999	7.16	18.25	
J080215.8-094214	J0802.3-0941	blazar	0.997	7.67	25.41	
J081338.1-035717	J0813.5-0356	blazar	0.995	29.42	17.09	
J082628.2-640416	J0826.3-6400	blazar	0.995	163.9	13.78	BLL (Peña-Herazo et al. 2017)
J082930.3+085820	J0829.3+0901	blazar	1	2.31	14.64	fsrq (4FGL, Collaboration 2019)
J084121.3-355505	J0841.3-3554	blazar	0.998	23.48	106.29	
J084831.8-694109	J0847.2-6936	blazar	0.996	13.47	10.77	
J092818.1-525700	J0928.3-5255	likely blazar	0.984	8.27	23.01	
J093754.5-143349	J0937.9-1435	blazar	1	3.27	17.61	BLL (Paiano et al. 2018a)
J095249.5+071330	J0952.8+0711	blazar	0.999	6.93	17.83	BLL (Paiano et al. 2018a), bcu (4FGL, Collaboration 2019)
J102432.6-454429	J1024.4-4545	blazar	0.999	29.91	13.23	
J103332.4-503527	J1033.4-5035	blazar	0.997	17.95	46.65	
J103755.1-242546	J1038.0-2425	likely blazar	0.929	4.12	11.79	bcu (4FGL, Collaboration 2019)
J104031.7+061722	J1040.4+0615	blazar	1	3	52.07	
J104503.3-594102	J1045.1-5941	pulsar	0.006	62.56	535.09	
J104939.4+154839	J1049.7+1548	likely blazar	0.985	6.99	15.92	bll (4FGL, Collaboration 2019)
J110506.3-611602	J1105.2-6113	blazar	0.9	3.15	93.04	pulsar (4FGL, Collaboration 2019)
J111715.1-533815	J1117.2-5338	blazar	0.999	7.26	44.36	
J111957.0-264322	J1119.8-2647	blazar	0.998	4.08	16.46	
J111958.9-220457	J1119.9-2204	pulsar	0.009	0.83	73.95	
J112504.2-580540	J1125.1-5803	likely blazar	0.988	22.21	23.27	
J112624.8-500807	J1126.8-5001	likely blazar	0.989	11.56	18.34	
J113032.6-780107	J1130.7-7800	likely blazar	0.985	141.8	30.49	
J113209.3-473854	J1132.0-4736	blazar	0.995	55.61	19.5	
J114141.7-140755	J1141.6-1406	likely blazar	0.988	23.8	18.48	BLL (Ricci et al. 2015), bll (4FGL, Collaboration 2019)
J114600.8-063851	J1146.1-0640	blazar	0.999	9.2	17.5	BLL (Paiano et al. 2017a)
J114912.0+280720	J1149.1+2815	blazar	0.993	1.88	9.01	
J115514.5-111125	J1155.3-1112	likely blazar	0.988	4.6	15.97	
J120055.1-143039	J1200.9-1432	likely blazar	0.987	7.9	14.25	bll (4FGL, Collaboration 2019)
J122014.4-245948	J1220.0-2502	blazar	0.996	27.69	12.96	
J122019.8-371414	J1220.1-3715	blazar	0.996	15.34	21.24	
J122127.4-062846	J1221.5-0632	blazar	0.993	3	30.99	QSO (Crespo et al. 2016a)
J122257.0+121439	J1223.2+1215	blazar	0.998	0.9	15.85	bcu (4FGL, Collaboration 2019)
J122336.8-303247	J1223.3-3028	blazar	0.999	25.72	13.94	
J122536.7-344724	J1225.4-3448	blazar	1	30.36	12.59	
J123140.3+482149	J1231.6+4825	blazar	0.995	2.87	10.31	fsrq (4FGL, Collaboration 2019)
J123204.2+165528	J1232.3+1701	blazar	0.996	2.55	17.76	bll (4FGL, Collaboration 2019)
J123235.9-372056	J1232.5-3720	blazar	0.999	4.6	20.22	
J123447.7-043254	J1234.7-0437	blazar	0.99	3.23	16.04	Sy2 (Paiano et al. 2017a)
J123726.6-705140	J1236.6-7050	blazar	1	5.23	20.21	
J124021.3-714858	J1240.3-7149	blazar	0.99	147.6	42.95	
J124919.5-280834	J1249.1-2808	blazar	0.995	34.16	24.57	
J124919.7-054540	J1249.5-0546	blazar	0.999	3.89	11.48	bcu (4FGL, Collaboration 2019)
J125058.4-494444	J1251.0-4943	blazar	0.993	2.77	25.55	
J125606.1-591931	J1256.1-5919	blazar	0.999	3.44	32.48	
J125949.4-374857	J1259.8-3749	blazar	0.993	3.45	27.85	BLL (Ricci et al. 2015)
J130059.5-814810	J1259.3-8151	likely blazar	0.988	3.48	16.65	
J131140.3-623314	J1311.8-6230	blazar	0.994	1.46	90.04	
J131552.8-073304	J1315.7-0732	blazar	0.998	21.83	42.6	
J132210.3+084230	J1322.3+0839	blazar	0.998	4.66	15.73	BLL (Crespo et al. 2016b), fsrq (4FGL, Collaboration 2019)
J132939.6-610735	J1329.8-6109	likely pulsar	0.059	4.26	82.45	
J134042.0-041009	J1340.6-0408	blazar	1	9.22	21.47	BLL (Paiano et al. 2018a), bll (4FGL, Collaboration 2019)

Table 1
(Continued)

Swift Name SwF3	Fermi Name 3FGL	Class	Random Forest Blazar Probability	X-Ray Flux[a] (0.1–2.4) keV	Gamma-Ray Flux[a] (0.1–100) GeV	Notes Classification in Literature
J134706.8-295843	J1346.9-2958	blazar	0.99	14.45	32.72	BLL (Ricci et al. 2015)
J135340.2-663958	J1353.5-6640	blazar	1	98.07	47.41	
J140514.7-611823	J1405.4-6119	likely pulsar	0.053	6.54	364.56	
J141133.3-072256	J1411.4-0724	blazar	0.997	4.55	15.79	BLL (Paiano et al. 2018a)
J141901.2+773229	J1418.9+7731	likely blazar	0.937	29.31	25.19	
J144544.5-593200	J1445.7-5925	blazar	0.996	23.37	57.41	
J151148.6-051348	J1511.8-0513	blazar	0.994	181.8	42.29	BLL (Paiano et al. 2018a)
J151150.9+662450	J1512.3+6622	blazar	0.997	17.77	8.45	
J151212.9-225507	J1512.2-2255	blazar	0.999	12.35	33.85	BLL (Peña-Herazo et al. 2017), bcu (4FGL, Collaboration 2019)
J151256.6-564027	J1512.8-5639	blazar	0.998	9.7	54.01	bcu (4FGL, Collaboration 2019)
J151319.0-372015	J1513.3-3719	blazar	0.993	3.99	15.38	
J151649.8+263635	J1517.0+2637	blazar	0.999	2.52	8.19	
J152603.0-083146	J1525.8-0834	blazar	0.995	4.21	11.27	BLL (Paiano et al. 2017a), bcu (4FGL, Collaboration 2019)
J152818.2-290257	J1528.1-2904	blazar	0.999	6.37	12.47	bcu (4FGL, Collaboration 2019)
J154150.1+141441	J1541.6+1414	blazar	0.999	3.38	16.37	BLL (Paiano et al. 2017a)
J154459.2-664148	J1545.0-6641	likely blazar	0.975	99.02	25.03	
J154946.4-304502	J1549.9-3044	blazar	0.997	14.11	20.16	
J154952.1-065909	J1549.7-0658	blazar	1	47.5	51.58	
J161543.0-444921	J1615.6-4450	likely blazar	0.985	8.98	26.6	
J162432.2-465756[c]	J1624.1-4700	likely pulsar	0.049	35.43	23.69	
J165338.2- 015837	J1653.6-0158	pulsar	0	1.29	128.17	pulsar (4FGL, Collaboration 2019)
J170409.6+123423	J1704.1+1234	blazar	0.994	24.13	18.82	BLL (Paiano et al. 2018a)
J170433.9-052841	J1704.4-0528	likely blazar	0.977	35.56	34.16	BLL (Paiano et al. 2018a)
J171107.0-432416	J1710.6-4317	blazar	0.997	13.67	38.93	
J172142.1-392205	J1721.8-3919	blazar	0.998	12.77	60.06	
J172858.2+604400	J1729.0+6049	blazar	0.995	3.82	8.46	
J173250.5+591234	J1732.7+5914	blazar	1	3.9	8.94	
J180106.8-782248[d]	J1801.5-7825	blazar	0.999	4.17	14.21	
J181720.4-303258	J1817.3-3033	blazar	0.993	15.26	18.63	
J182338.8-345413	J1823.6-3453	likely blazar	0.964	284.6	113.07	
J183539.5+135048	J1835.4+1349	blazar	0.992	3.13	14.56	bll (4FGL, Collaboration 2019)
J184230.1-584158	J1842.3-5841	blazar	1	105.9	32.46	
J184433.1-034627	J1844.3-0344	pulsar	0.005	1.21	197.44	pulsar (4FGL, Collaboration 2019)
J190843.2-012954	J1908.8-0130	likely pulsar	0.058	2.76	55	
J192114.1+194004	J1921.6+1934	likely blazar	0.964	15.13	26.68	
J192242.1-745355	J1923.2-7452	blazar	1	37.95	26.49	BLL (Peña-Herazo et al. 2017)
J193320.2+072620	J1933.4+0727	blazar	0.99	44.32	30.17	
J193420.1+600138	J1934.2+6002	blazar	0.996	7.35	15.7	bcu (4FGL, Collaboration 2019)
J194247.5+103327	J1942.7+1033	likely blazar	0.919	90.96	148.22	
J194633.6-540235	J1946.4-5403	pulsar	0.005	1.77	46.91	pulsar (4FGL, Collaboration 2019)
J195149.7+690719	J1951.3+6909	likely blazar	0.978	4.06	5.34	
J195800.3+243804	J1958.1+2436	blazar	0.996	24.16	24.55	
J200505.5+700437	J2004.8+7003	blazar	1	48.6	38.69	
J200635.7+015222	J2006.6+0150	likely blazar	0.965	4.13	24.17	pulsar (4FGL, Collaboration 2019)
J201431.1+064851	J2014.5+0648	blazar	1	20.16	35.62	
J201525.3-143205	J2015.3-1431	blazar	1	5.04	16.18	BLL (Crespo et al. 2016a)
J202154.9+062914	J2021.9+0630	blazar	0.996	2.36	27.83	BLL (Crespo et al. 2016b), bcu (4FGL, Collaboration 2019)
J203027.9-143919	J2030.5-1439	blazar	0.997	4.9	13.81	
J203450.9-420038	J2034.6-4202	blazar	0.999	15.01	20.59	
J203556.9+490038	J2035.8+4902	blazar	0.999	9.18	32.78	
J203649.6-332829	J2036.6-3325	likely blazar	0.955	45.79	16.75	BLL (Crespo et al. 2016a)
J203935.8+123002	J2039.7+1237	blazar	0.998	2.77	9.54	

Table 1
(Continued)

Swift Name SwF3	Fermi Name 3FGL	Class	Random Forest Blazar Probability	X-Ray Flux[a] (0.1–2.4) keV	Gamma-Ray Flux[a] (0.1–100) GeV	Notes Classification in Literature
J204312.6+171019	J2043.2+1711	pulsar	0.004	1.54	149.36	
J204351.5+103408	J2044.0+1035	likely blazar	0.923	4.5	16.94	bcu (4FGL, Collaboration 2019)
J205357.9+690518	J2054.3+6907	likely blazar	0.985	1.08	18.17	
J205950.4+202905	J2059.9+2029	likely blazar	0.983	5.04	8.43	
J210940.0+043958	J2110.0+0442	blazar	0.995	8.98	16.64	
J211522.2+121802	J2115.2+1215	blazar	0.996	3.59	15.16	
J211754.9-324329	J2118.0-3241	blazar	1	5.2	11.72	
J212729.3-600102	J2127.5-6001	blazar	1	20.1	10.02	bcu (4FGL, Collaboration 2019)
J212945.1-042907	J2129.6-0427	likely pulsar	0.091	1.91	30.86	pulsar (4FGL, Collaboration 2019)
J213348.6+664704	J2133.8+6648	blazar	1	7.14	57.88	
J214247.5+195812	J2142.7+1957	blazar	1	12.8	10.23	
J215123.0+415635	J2151.6+4154	blazar	0.996	18.46	38.15	
J220941.7-045109	J2209.8-0450	likely blazar	0.926	3.04	15.14	BLL (Paiano et al. 2017a)
J221532.1+513529	J2215.6+5134	pulsar	0.002	1.41	73.41	
J222911.2+225456	J2229.1+2255	blazar	0.99	54.31	13.32	BLL (Paiano et al. 2017a), bcu (4FGL, Collaboration 2019)
J224437.0+250344	J2244.6+2503	blazar	1	3.42	13.59	BLL (Paiano et al. 2017a)
J224710.1-000512	J2247.2-0004	blazar	0.99	0.72	26.93	BLL (Sandrinelli et al. 2013)
J225003.5-594520	J2249.3-5943	likely blazar	0.962	2.62	9.67	
J225032.7+174918	J2250.3+1747	blazar	0.991	1.98	15.86	BLL (Paiano et al. 2017a), bcu (4FGL, Collaboration 2019)
J230012.4+405223	J2300.0+4053	likely blazar	0.984	18.22	19.72	
J230351.7+555618	J2303.7+5555	blazar	0.995	30.74	23.73	
J230848.5+542612	J2309.0+5428	blazar	0.998	5.03	14.52	
J232127.1+511118	J2321.3+5113	blazar	1	5.73	11.7	
J232137.1-161926	J2321.6-1619	blazar	0.993	26.84	11.78	BLL (Paiano et al. 2017a)
J232938.7+610112	J2329.8+6102	blazar	0.996	44.15	29.13	
J233626.4-842650	J2337.2- 8425	blazar	0.997	6.73	14.16	BLL (Peña-Herazo et al. 2017)
J235115.9-760018	J2351.9-7601	blazar	0.997	7.98	17.73	BLL (Peña-Herazo et al. 2017)
J235825.0+382857	J2358.5+3827	blazar	1	20.47	18.5	Sy2 (Paiano et al. 2017a)
J235836.8-180718	J2358.6-1809	blazar	1	23.48	18.97	BLL (Paiano et al. 2017a)

Notes.
[a] Flux in the units of 10^{-13} erg cm^{-2} s^{-1}.
[b] Positionally coincident with a star, TYC 5993-3722-1.
[c] Positionally coincident with a rotationally variable star, CD-46 10711 of type K1IV(e).
[d] Positionally coincident with a star, HD162298 of type K4III.

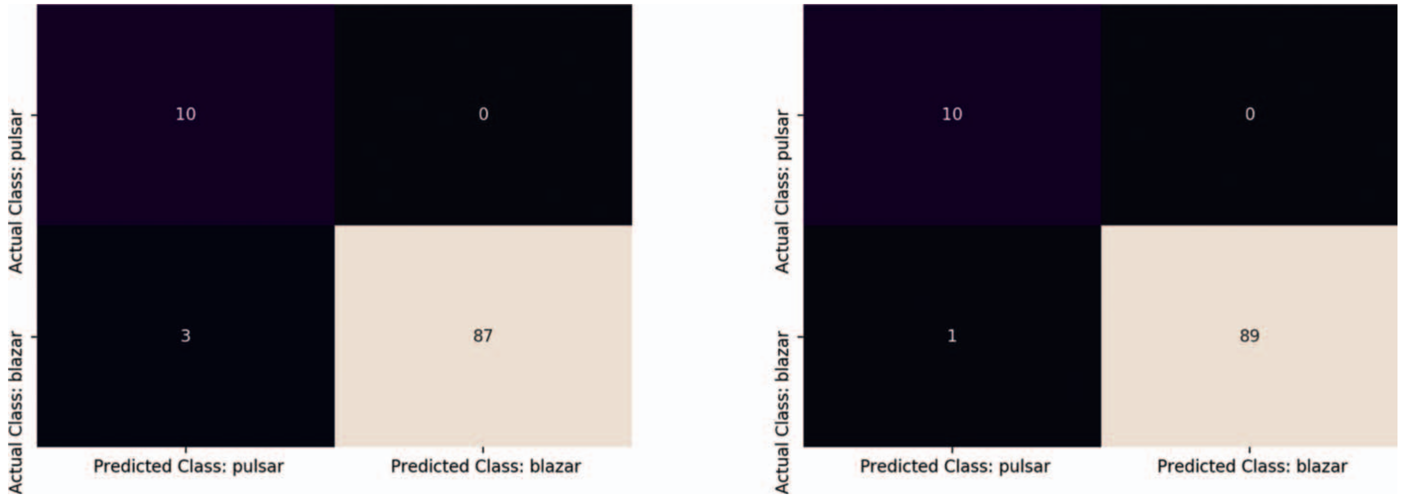

(a) Decision Tree (b) Random Forest

Figure 6. (a) Confusion matrix for test sample (100 sources: 90 blazars and 10 pulsars) for the decision tree classifier. As seen from the figure, the decision tree predicted all pulsars correctly, but three blazars were wrongly predicted as pulsars. The accuracy of this method was 97%. (b) Confusion matrix for the test sample of the random forest classifier. As seen from the figure, both the blazars and pulsars were correctly predicted by this method for 99 sources out of 100. Only one blazar was wrongly predicted as a pulsar in this case, yielding an accuracy score of 99%.

Table 2
Classification Using Machine Learning: Ambiguous Classifications

Swift Name SwF3	3FGL Name 3FGL	Random Forest Blazar Probability	Notes Classification in Literature
J052939.5+382321	J0529.2+3822	0.121	
J082623.6-505743	J0826.3-5056	0.198	
J083843.4-282702	J0838.8-2829	0.116	
J085505.8-481518	J0855.4-4818	0.14	
J085755.9-483424	J0858.0-4834	0.176	
J093444.6+090356	J0935.2+0903	0.692	
J112042.3+071313	J1120.6+0713	0.124	bcu (4FGL, Collaboration 2019)
J122758.7-485342	J1227.9-4854	0.417	XSS J12270-4859 (de Martino et al. 2015)
J125821.5+212352	J1258.4+2123	0.228	
J130832.0+034407	J1309.0+0347	0.59	
J141045.2+740505	J1410.9+7406	0.154	
J142035.9-243022	J1421.0-2431	0.348	
J154343.6-255608	J1544.1-2555	0.178	
J162607.8-242736	J1626.2-2428c	0.15	
J173508.3-292954	J1734.7-2930	0.255	
J175316.4-444822	J1753.6-4447	0.123	
J175359.6-292908	J1754.0-2930	0.106	
J180351.7+252607	J1804.1+2532	0.34	
J180425.0-085003	J1804.5-0850	0.874	
J181307.6-684713	J1813.6-6845	0.572	
J182914.0+272902	J1829.2+2731	0.131	bcu (4FGL, Collaboration 2019)
J182915.5+323432	J1829.2+3229	0.145	bcu (4FGL, Collaboration 2019)
J184833.8+323251	J1848.6+3232	0.73	
J185606.6-122148	J1856.1-1217	0.518	
J190444.5-070743	J1904.7-0708	0.77	
J201537.2+371119	J2015.6+3709	0.862	FSRQ (4FGL, Collaboration 2019)
J204806.3-312012	J2047.9-3119	0.781	bcu (4FGL, Collaboration 2019)
J212601.5+583148	J2125.8+5832	0.222	
J214429.5-563850	J2144.6-5640	0.614	BLL (Peña-Herazo et al. 2017)
J215046.5-174956	J2150.5-1754	0.504	BLL (Paiano et al. 2017a), bcu (4FGL, Collaboration 2019)
J225045.6+330515	J2250.6+3308	0.151	

5. Discussion and Conclusions

The main objective of this paper is to attempt to classify potential X-ray counterpart sources for the unassociated sample in the 3FGL catalog, which constitutes about one-third of the total source list. A complete classification of these mysterious gamma-ray sources is required for complete understanding of the high-energy universe. In this work, we utilize gamma-ray data in conjunction with X-ray data to classify these sources as either blazars or pulsars, because these two classes dominate the known sources in the *Fermi* catalogs. As already discussed, blazars can often be distinguished from pulsars based on just the gamma-ray and X-ray properties. We conduct a robust analysis by comparing a set of distinguishing parameters simultaneously using machine-learning techniques. This analysis yields ~79% blazars and 6% pulsars along with 14% ambiguous sources. This is roughly consistent with the known gamma-ray source population in the *Fermi* catalogs, and it has yielded several classifications of potentially new X-ray source associations with previously unassociated gamma-ray sources. From Table 1, it can be seen that 134 of the likely X-ray/gamma-ray counterpart sources are identified as ⩾99% likely to be a blazar, with 75 of these not previously discovered or classified. Similarly, out of the seven pulsars based on $P_{\rm bzr} \leqslant 1\%$, four are new candidates based on our algorithm and the other three are listed as pulsars in the 4FGL catalog.

It should be noted that this study does not take into account the presence of other source classes, such as supernova remnants, globular clusters, starburst galaxies, high-mass X-ray binaries, etc. It is indeed possible that some of the unassociated sources are neither blazars nor pulsars, in particular, the ones with blazar probabilities less than 90% and greater than 10% (see Table 2). In order to further confirm the classifications for these objects, in future work, we will (i) add more X-ray parameters derived from the spectral analysis, and (ii) utilize the information from other multiwavelength catalogs, e.g., *Wide-field Infrared Survey* point-source catalog (Cutri et al. 2013), NVSS (Condon et al. 1998), SUMSS (Mauch et al. 2003), ATCA (Petrov et al. 2013), and UVOT, along with the gamma-ray and X-ray properties. The multiwavelength studies for these objects will indeed confirm the nature of the underlying sources, which would fit them into either blazar or pulsar or "other" categories. The mysterious sources in the "other" category are excellent targets for more thorough investigations.

The authors would like to gratefully acknowledge the support provided by NASA research grants 80NSSC17K0752 and 80NSSC18K1730. This research has made use of the ZBLLAC spectroscopic library: http://www.oapd.inaf.it/zbllac. The astronomical tool to compare databases, Topcat (Taylor 2005), was employed in this work. We would like to thank Dr Eric Feigelson at Pennsylvania State University for the help and feedback in the implementation of the machine-learning methods.

Software: scikit-python (version 0.20.3, Pedregosa et al. 2011), Topcat (version 4.6-3, Taylor 2005).

Appendix
Pulsar Analysis from *Swift* Archival Data

Out of 59 pulsars used in our machine-learning algorithms, ten were obtained from *Swift* archival data. Their spectra were fitted with both power law and power law with exponential cutoff models using XSpec `version 12.10.0c`. The column densities for all the sources were calculated using the HEASARC column density calculator[7] and were fixed during the fitting procedure. The results from the best-fit models are provided Table 3 as shown below.

Table 3
Pulsars Analysis from the *Swift*-XRT Archival Data

3FGL	*Swift* OBS ID	N_H	Γ_X	β	Flux[a]	χ^2	d.o.f.
J0205.5+6448	00010028003	0.48	1.80 ± 0.15	...	0.21	9.35	10
J0437.2-4713	00080960001	0.01	2.85 ± 0.05	...	0.15	54.87	42
J0534.5+2201	00058970001	0.21	1.89 ± 0.03	...	641.41	303.54	171
J1119.1-6127	00081966001	1.09	1.41 ± 0.18	...	2.14	10.26	9
J1227.9-4854	00041135011	0.11	1.53 ± 0.16	...	0.28	2.48	7
J1509.4-5850	00080517002	1.66	1.61 ± 0.07	...	3.12	65.90	55
J1823.7-3019	00035341002	0.13	1.01 ± 0.007	...	21.32	1043.12	725
J1824.6-2451	00032785004	0.19	0.008 ± 0.14	3.55 ± 0.65	2.42	107.14	97
J1833.5-1033	00053600099	1.25	0.13 ± 0.16	2.38 ± 0.28	8.31	142.04	149
J2032.2+4126	00093148014	1.19	1.84 ± 0.23	...	0.44	1.96	6

Note.
[a] The flux range is 0.1–2.4 keV and units are 10^{-11} erg cm^{-2} s^{-1}.

[7] https://heasarc.gsfc.nasa.gov/cgi-bin/Tools/w3nh/w3nh.pl

ORCID iDs

Amanpreet Kaur https://orcid.org/0000-0002-0878-1193
Jamie A. Kennea https://orcid.org/0000-0002-6745-4790

References

Abdo, A. A., Ackermann, M., Ajello, M., et al. 2010, ApJS, 188, 2
Acero, F., Ackermann, M., Ajello, M., et al. 2015, ApJS, 218, 23
Ackermann, M., Ajello, M., Allafort, A., et al. 2012, Sci, 338, 1190
Ackermann, M., Ajello, M., Atwood, W. B., et al. 2015, ApJ, 810, 14
Breiman, L. 2001, Mach. Learn., 45, 5
Chawla, N. V., Bowyer, K. W., Hall, L. O., & Kegelmeyer, W. P. 2002, J. Artif. Intell. Res., 16, 321
Chiaro, G., Salvetti, D., La Mura, G., et al. 2016, MNRAS, 462, 3180
Condon, J. J., Cotton, W. D., Greisen, E. W., et al. 1998, AJ, 115, 1693
Crespo, N. Á, Massaro, F., Milisavljevic, D., et al. 2016a, AJ, 151, 95
Crespo, N. Á, Masetti, N., Ricci, F., et al. 2016b, AJ, 151, 32
Cutri, R. 2013, VizieR Online Data Catalog, 2328, 0
D'Abrusco, R., Massaro, F., Paggi, A., et al. 2013, ApJS, 206, 12
de Martino, D., Papitto, A., Belloni, T., et al. 2015, MNRAS, 454, 2190
Falcone, A. D., Pryal, M., Stroh, M., et al. 2015, in The 6th Fermi Symp., ed. B. Lott (NASA: Greenbelt, MD), https://fermi.gsfc.nasa.gov/science/mtgs/symposia/2015/program/wednesday/session12A/AFalcone.pdf
Fossati, G., Maraschi, L., Celotti, A., Comastri, A., & Ghisellini, G. 1998, MNRAS, 299, 433
Ghisellini, G., Righi, C., Costamante, L., & Tavecchio, F. 2017, MNRAS, 469, 255
Landoni, M., Massaro, F., Paggi, A., et al. 2015, AJ, 149, 163
Lefaucheur, J., & Pita, S. 2017, A&A, 602, A86
Li, K.-L., Kong, A. K. H., Hou, X., et al. 2016, ApJ, 833, 143
Marelli, M. 2012, PhD thesis, University of Insubria, arXiv:1205.1748
Marelli, M., Luca, A. D., & Caraveo, P. A. 2011, ApJ, 733, 82
Massaro, F., Álvarez Crespo, N., D'Abrusco, R., et al. 2016, Ap&SS, 361, 337
Massaro, F., D'Abrusco, R., Tosti, G., et al. 2012, ApJ, 750, 138
Mauch, T., Murphy, T., Buttery, H. J., et al. 2003, MNRAS, 342, 1117
Mirabal, N., Charles, E., Ferrara, E. C., et al. 2016, ApJ, 825, 69
Mirabal, N., Frías-Martinez, V., Hassan, T., & Frías-Martinez, E. 2012, MNRAS: Letters, 424, L64
Mukai, K. 1993, Legacy, 3, 21
Nolan, P. L., Abdo, A. A., Ackermann, M., et al. 2012, ApJS, 199, 31
Paiano, S., Falomo, R., Scarpa, R., Landoni, M., & Treves, A. 2017a, ApJ, 844, 120
Paiano, S., Falomo, R., Treves, A., Franceschini, A., & Scarpa, R. 2018a, ApJ, 851, 135
Paiano, S., Falomo, R., Treves, A., & Scarpa, R. 2018b, ApJL, 854, L32
Paiano, S., Landoni, M., Falomo, R., et al. 2017b, ApJ, 837, 144
Pedregosa, F., Varoquaux, G., Gramfort, A., et al. 2011, J. Mach. Learn. Res., 12, 2825
Peña-Herazo, H. A., Marchesini, E. J., Álvarez Crespo, N., et al. 2017, Ap&SS, 362, 228
Petrov, L., Mahony, E. K., Edwards, P. G., et al. 2013, MNRAS, 432, 1294
Pryal, M. 2015, BSc thesis, Penn State University
Quinlan, G. D., & Shapiro, S. L. 1990, ApJ, 356, 483
Ransom, S. M., Ray, P. S., Camilo, F., et al. 2011, ApJL, 727, L16
Ricci, F., Massaro, F., Landoni, M., et al. 2015, AJ, 149, 160
Salvetti, D., Chiaro, G., La Mura, G., & Thompson, D. J. 2017, MNRAS, 470, 1291
Sandrinelli, A., Treves, A., Falomo, R., et al. 2013, AJ, 146, 163
Saz Parkinson, P. M., Dormody, M., Ziegler, M., et al. 2010, ApJ, 725, 571
Saz Parkinson, P. M., Xu, H., Yu, P. L. H., et al. 2016, ApJ, 820, 8
Sharma, S. K., & Chauhan, R. 2011, CSci, 101, 308
Taylor, M. B. 2005, in ASP Conf. Ser. 347, Astronomical Data Analysis Software and Systems XIV, ed. P Shopbell, M. Britton, & R. Ebert (San Francisco, CA: ASP), 29
The Fermi-LAT Collaboration 2019, arXiv:1902.10045
Wu, J., Clark, C. J., Pletsch, H. J., et al. 2018, ApJ, 854, 99
Zyuzin, D. A., Karpova, A. V., & Shibanov, Y. A. 2018, MNRAS, 476, 2177